DOE/ER/45130--5

DE91 002396

II. RESEARCH PROGRESS
(Grant No. DE-FG02-84-ER45130)

Progress has been made on several fronts in the development and application of simplified energy and force functionals. These elucidate the basic features of bulk and defect structures, and are being coded in a form which can be used in atomistic simulations of materials properties. The main categories of materials which we have treated are transition metals, semiconductors, and aluminum alloys. We have analyzed the basic form of the angular dependence of the interatomic forces in these materials. We have then applied this understanding to the structures of polytetrahedrally packed transition metal compounds, icosahedral phases in the Ti–Mn system, and complex phases in Al–transition metal alloys. A force code for use in atomistic simulations of Si has also been developed. The Principal Investigator has completed a major review article on interatomic potentials for *Solid State Physics: Advances in Research and Applications*. The significance of the research accomplishments has also been recognized by several invited lectures, as well as a solicitation to write an article entitled *Cohesion (physics)* for the upcoming new edition of the McGraw-Hill Encyclopedia of Science and Technology.

A. Angular Forces in Transition Metals and Their Alloys
(Publications 1, 2, 3, 10, 11, 14, 15, and 17)

The use of the "embedded-atom" format[5,6] in many simulations of transition-metal defect properties has enabled the inclusion of physical effects which are usually incompletely included in interatomic potentials. The main such effect is the dependence of the effective bond strength between two atoms on the local environment. This leads naturally to positive surface tensions as well as inward relaxations of the top layers at surfaces. The embedded-atom format thus improves greatly on the pair-potential format, which does not naturally include such effects (although they can of course be artificially included by appropriately adjusting the pair potential). However, the embedded-atom format does not naturally obtain correct magnitudes or even signs for transition-metal structural-energy differences. For these it is necessary to include angular terms.

The generalization of the embedded-atom format to include angular terms is based on a moment analysis of the electronic density of states (DOS). The second moment, μ_2, describes the averaged width of the DOS, and is analogous to the local background density in the embedded-atom method. A treatment of the bonding energy based only on the second moment gives an energy functional having the embedded-atom format. By including[22] moments up to μ_4, one can describe the rudiments of the *shape* of the DOS. A small value of μ_4, at a fixed value of μ_2, corresponds to a bimodal density of states with well-defined bonding and antibonding peaks. This would be expected in a covalent bond. A large value of μ_4 implies that more of the weight is concentrated in the center of the band, with tails above and below the main part of the band increasing the values of the moments beyond μ_2. An extreme example of this type of behavior would be the quasi-Lorentzian shape that one expects from an impurity in a free-electron gas; we shall see later that transition-metal impurities in Al illustrate this. In general, one finds that the "covalent" shape for the DOS, with small μ_4, is favored for transition metals with half-filled d–bands. Nearly empty or filled d–bands favor large values of μ_4.

We have analyzed the geometric dependence of μ_4, and elucidated the resulting energetics, by calculating effective potentials associated with the moment description of the bonding energy. The most important contribution to the structural energies at this level is a four–body effective potential defined by

$$V_4^{\text{eff}}(\vec{R}_i,\vec{R}_j,\vec{R}_k,\vec{R}_l) = \frac{1}{4!}\,\mu_4(ijkl)\,\frac{\partial E_{el}}{\partial \mu_4}\bigg|_{\text{ref}} .$$

Here $\mu_4(ijkl)$ is the contribution to μ_4 from atoms (i–*l*), E_{el} is an approximation to the electronic binding energy based on the moments μ_0 through μ_4, and the derivative is evaluated for a particular "reference" environment. Potentials of this type are obtained by expanding the bonding energy in terms of the deviations of the various local environments in the system from the reference environment. Thus the potentials are environmentally dependent, and a single set of potentials cannot be used to treat a system with grossly differing atomic environments. The potentials depend strongly on the d–band filling, and change sign roughly at Groups IV and VI in a transition-metal row. In the half-filled d–band range, the four-body potential penalizes nearest-neighbor squares of atoms (*cf.* Fig. 1), while for the nearly empty and nearly filled ranges such squares are favored.

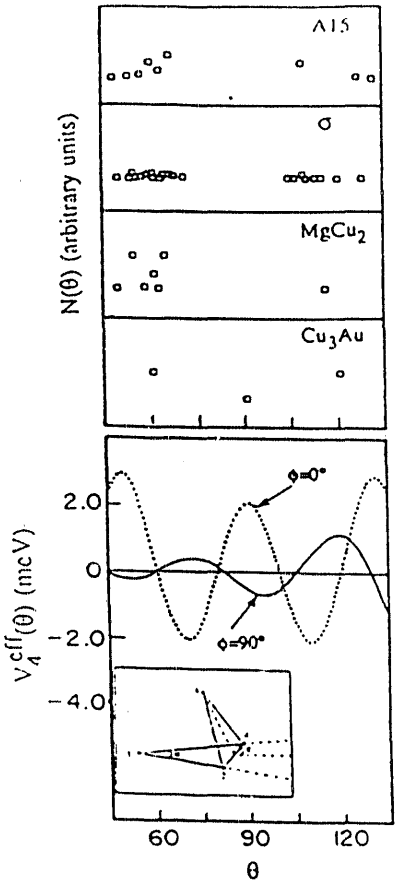

Figure 1. Four body potentials and angular histograms. Histograms show number of four-body clusters as function of angle θ for various structures (geometry defined in inset at bottom of figure). Also shown are plots of four-body potential for $\phi = 0°$ and $\phi = 90°$. Potentials obtained for roughly half-filled d–band.

We have applied these potentials to the structure of polytetrahedrally packed (PTP) transition-metal alloy and compound structures[23] (these are also referred to as Frank-Kasper structures). The PTP structures are built entirely of distorted tetrahedra, and are generally complex in that they have a large number of atoms per unit cell. Interest in these phases has increased recently because of their possible relevance to icosahedral phases. Our analysis, which is summarized in Fig. 1, shows that the dominant low-order angular contribution favoring the PTP structures over the fcc structure results from the preferential distribution of the angles in four–body clusters in regions where V_4^{eff} is negative. In particular, square nearest-neighbor clusters are uniformly avoided. These results are significant, because in most discussions of these structures it had been assumed that tetrahedral packing was universally preferred, at least locally, because it is the most *dense*. Our results show that even locally the preference is by no means universal, but is strongly dependent on the average d–band filling of the system. Other factors of course enter the stability as well, such as atomic size and the electronegativity difference between the constituents. However, for the non–Laves phases, we find that the electronic effects dominate, with the electronegativity difference essentially having the same effect as a small shift in the average d–band filling. In the Laves phases, we find that atomic-size effects are much more important, and are typically comparable to or larger than the electronic effects.

We have also begun to examine the energetics of various models of transition-metal based icosahedral phases on the basis of the energetic factors. (We have not yet completed a manuscript describing this work, but preliminary results were described at the March 1990 APS meeting in Anaheim.) The focus has been on the Ti–Mn system, because this is the most stable of the transition-metal based phases, and because this system has been intensively experimentally studied in–house by Professor Kelton's group. Our approach has been to generate plausible icosahedral-phase structures using "projection" techniques,[24] and to study their energetics using the tight-binding methodology. We have found that none of the proposed structures are energetically viable. They are at least several tenths of an eV per atom above the lowest-energy competing crystal structure. This is probably too large an energy difference to sustain a metastable state. In comparison, the heat of transformation[25] for the Al–Mn icosahedral phase to the competing crystalline structure is only 0.01–0.02 eV per atom. We have analyzed the problems of the proposed icosahedral phase structures. A large part of the destabilizing energy comes from the fact that a large number of atoms are simply undercoordinated or have neighbors that are too far away. This appears in our analysis as a value of μ_2 that is too small. The other major destabilizing contribution comes from angular environments of the Mn atoms. These have a large number of 90° bond angles, which our calculations show to be energetically unfavorable.

The angular-force calculations have been supplemented by a small number of *ab-initio* calculations using the augmented-spherical-wave method. The icosahedral phases cannot at present be treated with *ab-initio* methods so we have looked only at crystalline phases. We have found that at the Ti_3Mn stoichiometry (i–phase is roughly $Ti_{63}Mn_{37}$), the bcc–based Fe_3Al structure is preferred over the fcc–based Cu_3Au structure by 0.20 eV per atom. In comparison, our tight-binding methodology obtains 0.16 eV per atom. Both of these results are consistent with the formation of a bcc solid solution at the Ti end of the Ti–Mn phase diagram. In addition, we have found that in the Fe_3Al structure, the Mn sites do not have a magnetic moment. This is remarkable, given the strong tendency of Mn to form moments. However, the theoretical predictions are

confirmed by the NMR data given in *Publication 14*, which show no magnetic moments in the bcc solid solution, the icosahedral phase, or the complex structures that result from annealing the icosahedral phase.

B. Angular Forces in Semiconductors

(Publications 4, 6, 10, 13, 16, and 19)

As mentioned in the Introduction, a very large number of angular-force methods for Si have been developed over the past few years. These have included both methods based completely on interatomic potentials, and formulations[26–28] closer to the embedded-atom format, with high-order interactions of a restricted form automatically included. However, the discrepancies between schemes based on different assumed functional forms, and different input data, are very large. Different potentials attempting to describe Si can differ by as much as an order of magnitude. For this reason, theoretical analysis is necessary in order to establish the *functional form* of the angular forces. This analysis is similar to the moment analysis described above in connection with transition metals. Recent work by Harrison[10] has also used the moment method, but in a somewhat different format. Given the theoretical analysis, on can hope either to construct a completely *ab-initio* interatomic-potential description, or to construct a parametrized scheme based on a functional form with quantum-mechanical justification. We have opted for the latter route. We have used a generalization of the tight-binding moment methodology discussed above in connection with transition metals to develop a semi-empirical angular force scheme for Si. We have also evaluated the accuracy of this scheme by calculating several important materials parameters and comparing the results to *ab-initio* and experimental results, and to those of other angular-force methods.

It was necessary to generalize the moment method somewhat relative to the transition-metal case in order to treat the "covalent-metallic" transition[27] in Si. By this terminology it is meant that for a coordination number not exceeding four, a Si atom can form fairly independent bonds to its neighbors, as one would expect from a covalent material. For larger coordination numbers independent bonds cannot be formed. In the moment methodology discussed above, there is no possibility for independent bonds even at low coordination numbers, since all bonds interact. The covalent-metallic transition is not as readily noticeable in transition metals because the coordination number is seldom low enough, but it may still be important when treating energies of small fragments or dimer molecules.

In our treatment of the covalent-metallic transition, the scalar second moment of the DOS, μ_2, is replaced by a matrix moment $\underline{\mu}_2$. This is defined by

$$\mu_2^{\alpha\beta}(i) = \sum_{\gamma, j \neq i} h_{ij}^{\alpha\gamma} h_{ji}^{\gamma\beta}$$

where the $h_{ij}^{\alpha\beta}$ are interatomic couplings between s– and p–like orbitals. Thus $\underline{\mu}_2$ is a four-by-four matrix. The advantage of this matrix is that it describes the angular character of the local atomic environment although it is given entirely in terms of pair contributions. For example, the s–p part of the matrix vanishes in environments having inversion symmetry, but not in general otherwise; the p–p part of the matrix describes tetragonal or orthorhombic vs. cubic symmetry.

The energy associated with Ω_2 is given by

$$E_{el}^{(2)} = -\mathrm{Tr}[\Omega_2]^{1/2}$$

where $\mathrm{Tr}[\Omega_2]^{1/2}$ denotes the sum of the square roots of the eigenvalues of Ω_2. This form of the electronic bonding energy can obtain independent bond behavior for low coordination numbers. The eigenvalues correspond, roughly, to the strengths of the bonds to the neighboring atoms. If one starts with the ideal diamond structure, each broken bond at, for example, a vacancy or a surface, results in an eigenvalue that is close to zero. Thus the bonds act roughly independently. This yields a vacancy-formation energy which is close to the cohesive energy; scalar second-moment schemes typically yield vacancy-formation energies which are much smaller, and too small to be physical. For large coordination numbers, the matrix Ω_2 method no longer produces independent bonds, and the results are more similar to metallic bonding.

The total energy functional includes the Ω_2 term, a repulsive pair-potential term, a term describing the effects of μ_4, and an additional term describing the self-energy of the electrostatic dipole that is induced by an environment lacking inversion symmetry. Altogether, there are eight parameters. Six of these describe the energy and length scales of the s– and p–orbitals and the short-ranged repulsion. The remaining two parameters describe the μ_4 and electrostatic-dipole contributions. The values of the parameters were obtained by fitting to an *ab-initio* database including cohesive energies, bulk moduli, vibrational properties, and the unrelaxed vacancy-formation energy. Although the energy functional is rather complex for visualization purposes, a simpler picture can be obtained by calculating effective potentials in the same manner as was discussed above for transition metals. Using as a reference medium the ideal diamond structure, the angular potential shown in Fig. 2 is obtained. As is seen in the Figure, the form of the potential is quite similar to the "war-horse" Stillinger-Weber potential.[29] Thus there is *ab-initio* justification for potentials of this form. The calculated potential has a smaller magnitude than the Stillinger-Weber potential, but the discrepancy is small in comparison with the order-of-magnitude deviations between potential schemes that were discussed above. The present scheme differs from the Stillinger-Weber scheme in that the angular potential is environmentally dependent, and in the presence of four-body terms. These, as in the transition-metal case, penalize nearest-neighbor square arrangements of atoms, and are important in favoring the diamond structure over more closely packed structures.

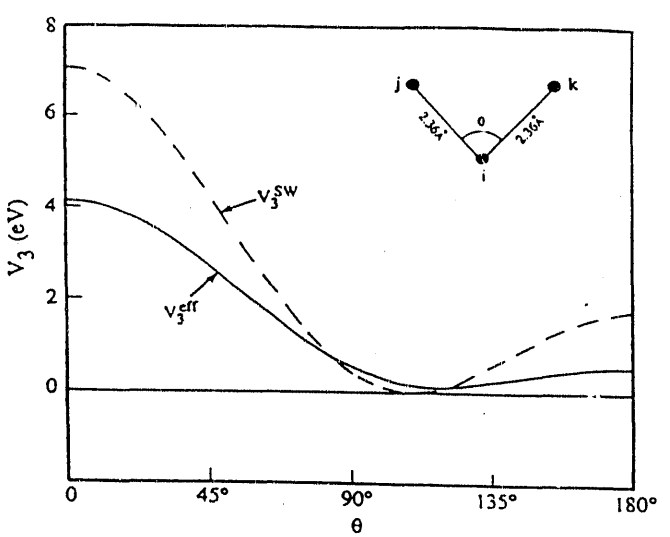

Figure 2.
Effective three-body potential V_3^{eff} obtained from our functional vs. angle θ. Stillinger Weber potential also included for comparison.

We have evaluated the accuracy of the potential by calculating the bcc–fcc energy difference, the internal-strain parameter η for the elastic constant C_{44}, and the hexagonal-site and tetrahedral-site interstitial formation energies and relaxations. The results are roughly as good as those of the best empirically fitted schemes. The primary weakness is that the estimate of η is too large, which results in a value of C_{44} over 50% too small. This suggests that the angular part of the forces is still too weak. In addition, the tetrahedral-site interstitial energy is too low by roughly a factor of two; the hexagonal-site interstitial energy is in agreement with the *ab-initio* results to within the accuracy of the latter. The low tetrahedral-site value is probably also due to the weakness of the angular forces. Overall, the results indicate that the format developed is a promising one for treating diamond-structure semiconductors, and a few "iterations" can be expected to produce considerably improved accuracy. Possible modifications we will investigate to improve the accuracy of the method will be described under Proposed Research.

C. Structures of Aluminum Alloys and Compounds

(Publications 5, 7, 8, and 18)

We have treated the energetics associated with both changes in the geometric packing arrangements of the atoms, and substitutional rearrangements characteristic of solid solutions.

1. *Complex structures of Al-transition metal compounds.* These have been of great interest lately because of their possible connection to icosahedral (i–) phases. A natural question to ask about these structures is whether their complexity is due to competing short-range interactions whose constraints cannot be simultaneously satisfied in any simple structure (the "ANNNI" scenario[30]), or whether there is a component of the energy which favors complexity in itself, and thus involves longer-ranged interactions caused by, for example, Fermi-surface effects. In an attempt to begin to answer this question, we have calculated the structural energy differences between the prototypical complex $Al_{12}W$ structure and the simpler competing Cu_3Au structure, for all of the 3d and 4d transition metals. The *ab-initio* augmented-spherical-wave code[31] was used for the calculations. The calculated energy differences (*cf.* Fig. 3) have a magnitude on the order of an eV, are largest for transition metals with half-filled d-bands, and are larger for the 4d transition metals than the 3d metals. These observations argue against atomic-size interpretations of the structural stability, which have much smaller energy differences and display different chemical trends. (Several of the transition metals have negative values of ΔE, but still do not form the $Al_{12}W$ structure. In these case, another structure forms which has energy lower than both the $Al_{12}W$ and Cu_3Au structures. For example, the energy of the DO_{22} structure for Al_3Nb is believed[32] to be 0.8–1.0 eV below that of the Cu_3Au structure, placing it slightly below the $Al_{12}W$ structure.)

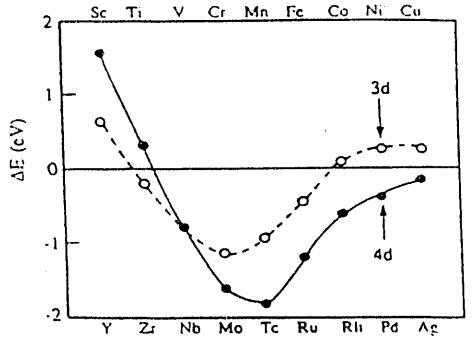

Figure 3.
Energy difference between $Al_{12}W$ and Cu_3Au structures.
$\Delta E = E(Al_{12}T) - E(Al_3T) - 9E(Al)$.

We find that a large part of the structural stability can be related to the shape of the d–projected DOS in the two structures. In the Cu_3Au structure, a very high peak is seen at the center of the band. This peak is due to non-bonding d–states, and suggests a Fermi-surface instability. It is eliminated in the $Al_{12}W$ structure and is, in fact, replaced by a dip or quasi-gap in the DOS. This effect leads to a large contribution stabilizing the $Al_{12}W$ structure for transition metals with nearly half-filled d–bands. Using a simplified square-band model of the DOS, we have estimated that the contribution of the non-bonding peak accounts for roughly 60% of the *ab-initio* structural energy differences.

The origin of this peak is precisely the high symmetry of the structure. Using an Anderson-lattice model, we have shown that the peak results from an approximate decoupling of certain d–Bloch waves from the free-electron continuum. This decoupling, in turn, is directly associated with the small unit cell size and high rotational symmetry of the Cu_3Au structure. In the $Al_{12}W$ structure, the unit cell size is more than three times larger, and the rotational symmetry is reduced (the icosahedron has higher symmetry than cubic, but the intersection of the icosahedral group and the cubic group of the Bravais lattice is smaller than the cubic group). Thus the non-bonding peak should be reduced or eliminated in this structure. We have found that the energy due to the non-bonding peak is approximately equally distributed between long-ranged and short-ranged effects. The former are related to the unit cell size. The latter can be approximately described by an angular potential surrounding the Mn atoms, which has a maximum at 90° bond angles.

It is interesting to note that all of the structures formed by Al–rich compounds with nearly half-filled d–band transition metals have large unit cell sizes and reduced rotational symmetry. Therefore the non-bonding peak effects should be reduced or eliminated in these as well, stabilizing the structures. In addition, our analysis of the distribution of Al–Mn–Al bond angles in these compounds has indicated an avoidance of 90° angles, consistent with the type of angular potential mentioned above. Finally, the physics of these structural energies may be relevant to i–phases as well. These have no exact translational symmetry, and with the exception of possibly a few sites, have no exact rotational symmetry either. These characteristics should help to stabilize the icosahedral structure relative to simpler competing structures such as the Cu_3Au structure. In fact, our calculations, together with measured transformation energies, suggest that the icosahedral structure lies roughly 0.8 eV per Mn atom *below* the Cu_3Au structure in energy (with appropriate amounts of Al included in the comparison to make the compositions equal). Although the broad range of systems which form i–phases suggests that the factors discussed here are not essential, they likely enhance the metastability of binary Al–transition metal i–phases with nearly half-filled d–bands.

2. *Al-transition metal solid solutions.* We have obtained a physical understanding of the chemical trends in effective Ising interactions for Al–transition metal alloys that were calculated in the preceding grant period. In addition, we have used them to study the solid-solution regions of the corresponding phase diagrams. The two most noticeable properties of the calculated values of the pair Ising interaction V_2 are that it is large and positive (corresponding to exothermic heats of formation) for all of the transition metals with partly-filled d–bands, and that it displays a pronounced minimum for the metals with half-filled d–bands. The exothermic values of V_2 are due to the high electron density of Al. This enhances the d-state resonant broadening at the Fermi level, for two reasons. First, the Fermi-level density of states DOS is increased by the high electron

density. Second, the Fermi wave vector is increased, which reduces the characteristic wavelength of the free-electron wave functions at the Fermi level, and thus enhances the s–d hybridization matrix element. In a picture based on Fermi's Golden Rule, the resonant width is proportional to the DOS and the square of the matrix element, and is thus strongly enhanced by a high background electron density. Support for this picture comes from the observed heats of formation[33] for transition metals with Mg, Al and Si. With increasing valence, the heats of formation become more exothermic for all of the cases for which systematic data exist; in fact, with Mg, the heats of formation are usually sufficiently endothermic that compounds do not form.

The presence of the minimum in V_2 for half-filled transition-metal d-bands may be traced to differences in the characteristic shape of the DOS in the Al host, as compared with the elemental transition metal. Elemental transition d–bands (*cf.* Fig. 4) are usually fairly well described via "square bands", with no dominant peaks near the center of the band. On the other hand, in the Al host, the DOS has a more Lorentzian shape, with pronounced tails. The Lorentzian shape has a somewhat destabilizing effect for nearly half-filled d–bands, resulting in less exothermic values of the heat of formation. This corresponds to reduced values of V_2.

We have used the calculated Ising interactions to evaluate heats of solution, solid solubilities, and short-range order parameters. (For the short-range order, we actually evaluated an effective potential which is a linear combination of the pair and multi-atom terms. This can be compared to "measured" potentials that are obtained from short-range order experiments.) The heats of solution are typically within 20% of the experimental values; the reason for this good agreement is probably the large energy scale of the heats, which are of order 1–2 eV per transition-metal atom. The solubilities were expressed in terms of energy differences between the solid solution and the competing crystal structure. The calculated energy differences (*cf.* Fig. 5) agree with experiment to within roughly 40%, and reflect the universal trend in Al–transition metal systems that the solubility at the Al end is greater than that at the transition-metal end of the phase diagram. Surprisingly, this effect was not well correlated with the asymmetry in the heat of solution. It was, however, strongly influenced by the energies of the competing ordered structures. The values of the short-range order effective potential were within 40% of experiment where reliable data exists.

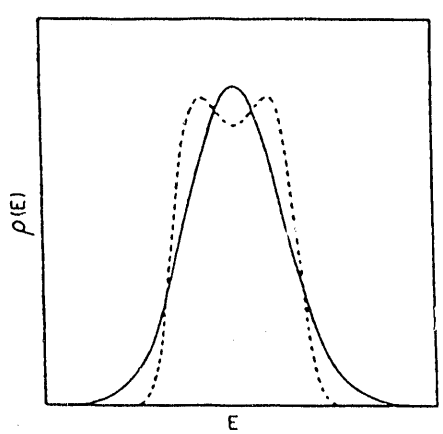

Figure 4. Model electronic d-band density of states for pure transition metal (dashed curve) and transition metal in Al host (solid curve).

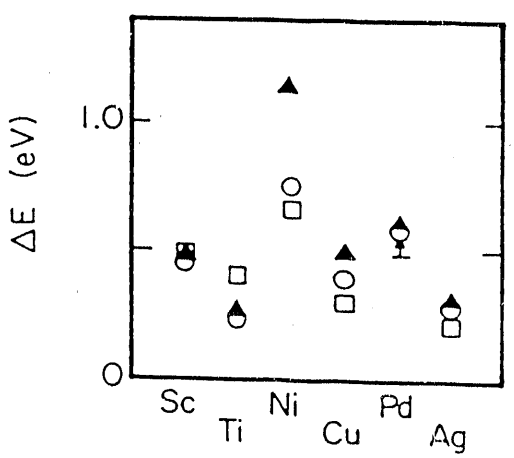

Figure 5. Solid-solubility energies for transition metals in Al host. $\Delta E = -k_B T \ln C_{max}$, where C_{max} is solid solubility. Squares denote experimental values, circles denote calculated values, and triangles denote calculated values in absence of lattice-relaxation effects.

3. *Al-Li alloys.* This work was motivated by the promising applications of these alloys in the aerospace industry. The goal was to develop an interatomic-potential scheme which could be used in atomistic simulations of solidification, transformations, and defect properties. This system is difficult to treat because of the large valence difference between the two constituents, which leads to large long-wavelength components in the pseudopotential seen by the electrons, and also because of the strong nonlocality of the Li pseudopotential. Both of these render standard pseudopotential expansion methods for generating effective potentials difficult to apply. We devised two modifications to the standard methods in order to treat these problems. First, instead of using a uniform positive background as a starting point, we used a background with a varying charge density corresponding to the local alloy composition. This reduced the magnitude of some of the long-wavelength components of the remaining part of the pseudopotential. Second, an approximate treatment of the nonlocality was developed, which utilized a nonlinear functional of the local charge density. These two improvements led to greatly improved values of the heats of solution and compound formation, whose magnitudes are generally underestimated by standard pseudopotential techniques. A correct ordering was also obtained for three competing structures at the 50% stoichiometry. However, the metastable Al_3Li compound in the Cu_3Au structure was actually predicted to be stable. This precludes the accurate calculation of a phase diagram. In addition, the Al_4Li_9 structure was found to have too high an energy to be stable. Clearly, these problems must be overcome if quantitative calculations are to be performed. However, for the purposes of atomistic defect calculations, the scheme that we have devised appears to be a useful compromise between accuracy and practicality.

D. Basic Theory of Interatomic Potentials in Condensed Matter
(Publications 9 and 12)

Our focus here has been on making more precise the nature of interatomic potentials which are "measured", in the sense that they are obtained from experimentally observed interatomic correlation functions, or from *ab-initio* total-energy calculations. We have emphasized short-range order properties in solid solutions. In the last few years, the mathematical machinery[34,35] has been developed for extracting uniquely defined, separation-dependent effective Ising interactions for these systems from experimentally obtained short-range order parameters. The machinery, known as the "Inverse Monte Carlo" method, uses successive spin flips to achieve a computer sample which has the same pair short-range order as the physical sample. It is then possible to establish the Ising interactions which would have been needed in a "forward" Monte Carlo calculation to produce this short-range order. One is then left with the question of what such Ising interactions mean. If the energetics were rigorously described by pair Ising interactions, then the inverse Monte Carlo parameters would be exactly equal to these. However, in general one believes that three–body and higher-order interactions make important contributions to the short-range order. Our aim was to establish how these interactions enter the "measured" Inverse Monte Carlo parameters.

We addressed this question by treating a simple model alloy containing nearest-neighbor interactions up the four–body level. The parameters were chosen to reproduce some aspects of the Cu–Au phase diagram, but do not precisely describe any known physical system. The short-range order in this model was established by exhaustive Monte Carlo simulations at several temperatures and compositions. Then the accuracy of several methods for obtaining effective pair Ising interactions from the many-body interactions was evaluated, by calculating the short-range order resulting from the pair

interactions, and comparing it to the full cluster model results. Beyond simply ignoring the higher-order terms, the simplest pair interactions were obtained by an averaged treatment of the higher-order terms, using higher-order correlation functions appropriate for essentially infinite temperature. Pair Ising interactions of this type are concentration-dependent, and are guaranteed to produce the correct short-range order at very high temperatures; however, these temperatures are usually above the alloy's melting point. In our case, we found errors of 50% or more in some cases at the order–disorder temperature. A much improved set of pair Ising interactions was found by including a possible temperature dependence; these interactions contain terms proportional to $V_2^{eff}V_3^{eff}/k_BT$, and other combinations of the various V_n^{eff}, where n is the order of the interaction. At the order-disorder temperature, this type of interaction produces errors of less than 20% (*cf.* Fig. 6).

It was concluded that the types of Ising interactions which are "measured" experimentally probably have the character of this last type of calculated parameter. This suggests that one might be able to obtain an experimental handle (otherwise very hard to obtain) on the magnitudes of the three-body and higher-order interactions by evaluating the environmental dependence of the measured parameters. We have obtained explicit formulas for both the compositional and temperature dependence. If either of these are important, then multi-body interactions must be included in the energetics of the system under consideration.

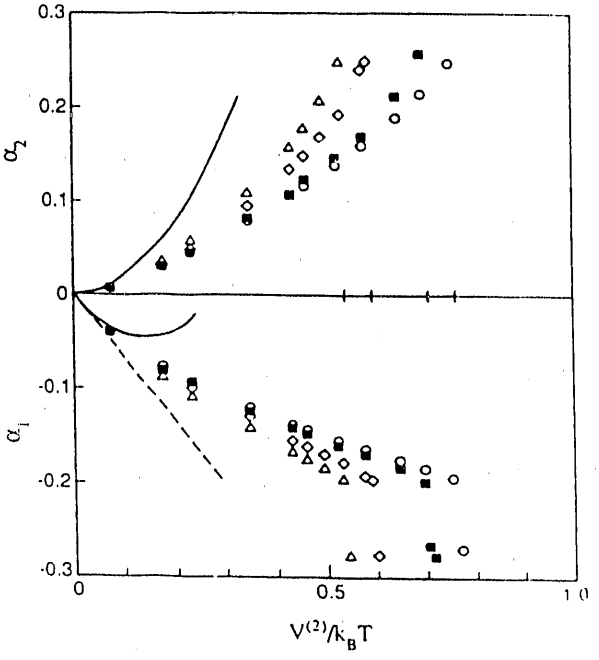

Figure 6. Short-range order parameters, at first (α_1) and second (α_2) neighbor distances. $V^{(2)}$ = 30 meV.
Solid squares: full cluster Hamiltonian.
Triangles: bare pair interaction only.
Diamonds: concentration-dependent interaction $V^{(2),eff}$.
Circles: concentration- and temperature-dependent interaction $U^{(2),eff}$.
Dashed and solid lines denote first- and second-order expansions in inverse temperature, respectively. Transition temperatures for the various models indicated by marks on the horizontal axis.

DISCLAIMER

END

DATE FILMED

11 / 27 / 90